Distributed Spintronic/CMOS Sensor Network for Thermal-Aware Systems

Abdelrahman G. Qoutb, *Student Member, IEEE*, and Eby G. Friedman, *Fellow, IEEE*

***Abstract*— Recent developments in IC technology rely on device scaling and 3-D integration, resulting in billions of devices compacted into a small area. These trends degrade the lifetime and reliability of the system due to an increase in temperature caused by high power densities. Dynamically managing a system based on the thermal characteristics is important to mitigate this issue. An on-chip thermal-aware system composed of hundreds of distributed thermal sensors is proposed. A hybrid spintronic/CMOS-based thermal sensor is described that exploits the thermal response and small area of an antiparallel magnetic tunnel junction. The sensor cell consumes as little as 500 pJ to read 1024 thermal sensor nodes and generates a thermal map of a system composed of 32 × 32 thermal sensors. The sensor cell exhibits a thermal linearity (R^2) up to 0.983 and a thermal sensitivity of 1.91 mV/K over the commercial temperature range of 0 °C to 85 °C while consuming 32 μW.**

***Index Terms*— Magnetic tunnel junction (MTJ), spintronic, thermal-aware system, thermal management system, thermal sensor.**

I. Introduction

TWO primary methods are used to achieve next-generation integrated systems, a large number of deeply scaled devices and die stacking. High power densities and thermal issues such as long heat conduction paths are produced, which, in turn, can dramatically degrade performance, reliability, and system robustness while increasing leakage currents [1], [2]. To manage the system workload and protect the system from overheating, methods such as allocating heat conduction paths and specialized cooling systems are used [3], [4]. These systems need to be supported with a temperature-aware capability to allocate and properly respond to critical hot spots.

A thermal-aware system can be achieved by distributing a large number of on-chip thermal sensors. These on-chip thermal sensors should be small in size, low power, high speed, temperature sensitive, and accurate over a wide temperature range. The on-chip thermal sensors should be appropriately placed to capture local hot spots. The location of the thermal sensors depends upon the sensor characteristics, system requirements, IC package, and cooling techniques [5].

Manuscript received August 21, 2019; revised January 14, 2020 and February 12, 2020; accepted March 13, 2020. Date of publication April 9, 2020; date of current version June 1, 2020. This work was supported in part by the National Science Foundation under Grant CCF-1716091, in part by Intelligence Advanced Research Projects Activity (IARPA) under Grant W911NF-17-9-0001, in part by Cisco Systems, in part by Qualcomm, in part by Synopsys, and in part by Google. *(Corresponding author: Abdelrahman G. Qoutb.)*

The authors are with the Department of Electrical and Computer Engineering, University of Rochester, Rochester, NY 14627 USA (e-mail: a.qoutb@rochester.edu; friedman@ece.rochester.edu).

Digital Object Identifier 10.1109/TVLSI.2020.2981443

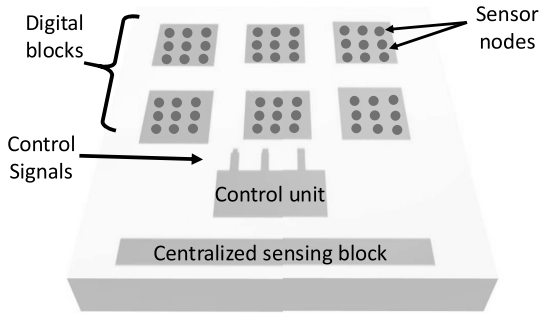

Fig. 1. Distributed thermal network system.

A small number of thermal sensor nodes are typically located around an IC, particularly near potential hot spots to support a thermal-aware system. For instance, Intel utilizes one thermal sensor per core in the Xeon 5400 series [6], while 25 thermal sensors are embedded in the IBM POWER6 processor [7]. The use of a few thermal sensors, however, limits the ability to fully monitor the significant spatial and dynamic temperature variations across an integrated system [8]. Thermal-aware systems manage the locally distributed thermal sensor nodes around an IC, dynamically controlling the system workload [8]–[10]. These systems, however, utilize a software-based management system which do not respond to individual thermal sensor nodes. In addition, the response time of these software solutions is long and consumes significant power, and hence hardware solutions are desirable. In this article, an integrated system to support a thermal-aware capability, as shown in Fig. 1, is proposed, where multiple thermal sensor nodes are distributed across an IC.

The distributed thermal sensor nodes communicate with a centralized sensing unit which collects temperature information from the individual sensor nodes, producing a thermal map of the system. A hybrid spintronic/CMOS-based analog thermal sensor is proposed here where the high temperature sensitivity of the magnetic tunnel junction (MTJ) antiparallel (AP) resistance is exploited, as illustrated in Fig. 2. The sensor output is compared with a reference source, as shown in Fig. 3 [4]. The analog thermal sensor behaves as a threshold temperature-based sensor, triggering a signal if the temperature (or voltage) exceeds a certain reference temperature (or voltage).

Several documents discuss thermal sensors using spintronic technology [11], [12]. In [11], a patent describes the use of an MTJ as a thermal sensor by sensing the change in the

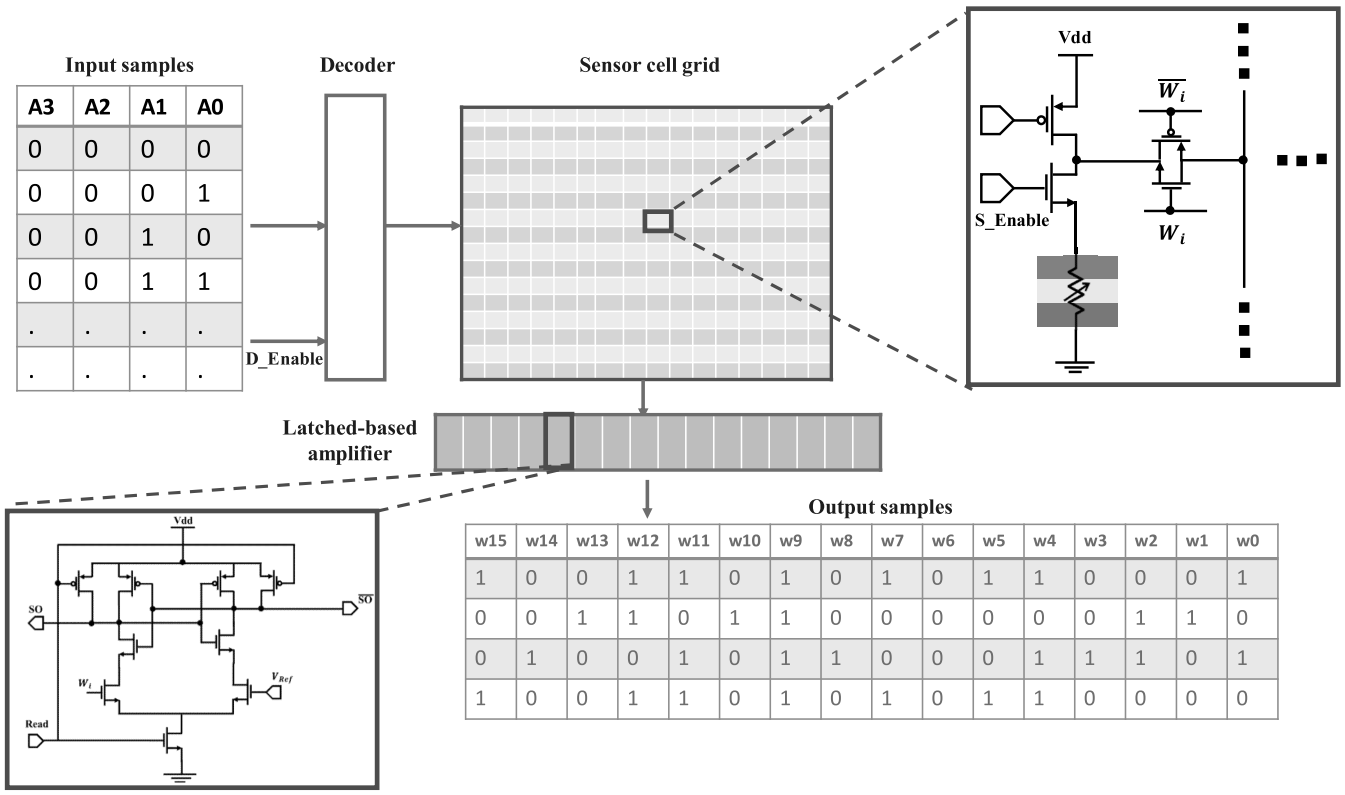

Fig. 2. Proposed thermal-aware system. The system input chooses the row being read through a decoder. The decoder enables the transmission gate of the sensor cell to the read line. The read lines are connected to a latched-based amplifier which produces the system output.

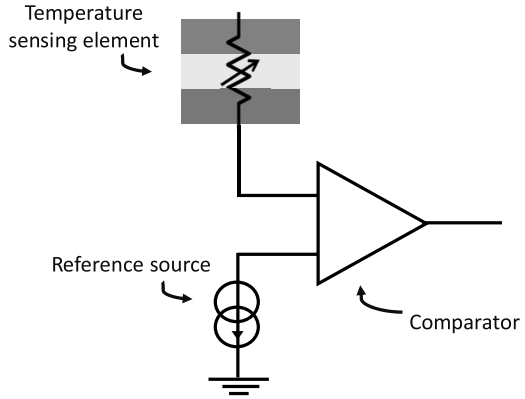

Fig. 3. On-chip analog thermal sensor.

resistance of an MTJ to temperature. Chung *et al.* [11] do not describe a thermal sensor, guidelines for using an MTJ as a thermal sensor, or the distinctive behavior of the P and AP resistance of an MTJ to temperature. In [12], the influence of temperature on the probability of device switching is noted. Sensing a change in the switching probability requires additional circuitry. In this article, the temperature is measured by a change in the AP resistance.

The proposed system includes a network of thermal sensor nodes distributed around an IC and additional circuitry, as described in Section II, that manages and controls the sensor signals and hence the system performance, as schematically shown in Fig. 1. This article is organized as follows. The proposed thermal-aware system is described in Section II, where the system architecture and circuit requirements are discussed. The use of an MTJ as a thermal sensor is discussed in Section III. In addition, a comparison between a CMOS diode and transistor-based thermal sensor with an MTJ/transistor temperature sensor is also provided in Section III. Simulation results are presented in Section IV followed by the conclusions in Section V.

II. Distributed Thermal Network

The proposed thermal-aware system is a network of thermal sensor nodes communicating with a control unit that collects temperature data and produces a thermal map. This thermal network provides the monitored system with dynamic real-time thermal information. The proposed system architecture, read and data signaling, and related circuitry are discussed below. The system components are described in Section II-A, the system signaling is illustrated in Section II-B, and the fabrication characteristics of the system are reviewed in Section II-C.

A. System Architecture

The proposed system architecture, as shown in Fig. 2, is managed as a memory grid, where the sensor nodes are organized in a grid-based topology. To read a system of $m \times n$ sensor nodes with m columns and n rows, a $\log_2 n - \text{to} - n$ decoder and m amplifiers are required. The input to the system decoder identifies the row being read. Each row shares the

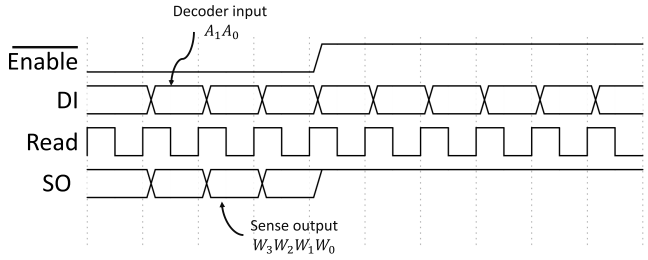

Fig. 4. System waveforms.

same enable signal, while each column shares the same bitline. The enable signal, generated from the system decoder, passes the sensor node voltage to the bitline and is read through a sense amplifier. The proposed sense amplifier is latch-based, composed of two inverters controlled by a read signal. The sensor node voltage is compared with a reference voltage that sets a threshold temperature. The system output is in a binary format indicating whether the state of the sensor node is either below or above a threshold voltage.

B. System Read and Data Signaling

The sequence of operations is as follows. During each read cycle, the enable signal controls the decoder to individually select one row. The output of each cycle is a vector of m sensor node reads. During each cycle, one row is read and n cycles are required to read n rows. The system input is generated from a counter, and the system output is stored within a memory.

An example of the data signal waveform of a 4×4 data signal is shown in Fig. 4. The decoder and sensor nodes are enabled by the enable signal, where the decoder input data are annotated as $A0$ and $A1$. The output of the decoder enables the individual transmission gates. Each transmission gate connects the associated sensor node output to the bitline. The read signal enables the sense amplifier to latch a bitline. In comparison with a reference voltage, the amplifier output is latched to either high or low. The output signals, $w0$, $w1$, $w2$, and $w3$, indicate the temperature status. By turning off the enable signal, the system saves energy by isolating the power from the sensor nodes and decoder.

The output of a distributed thermal network composed of 16×16 sensor nodes is illustrated in Fig. 5(b). The binary thermal map, as shown in Fig. 5(a), reflects the location of the individual sensor nodes. The thermal map indicates if the temperature is above or below a predefined threshold temperature and hence determines in real-time the location of the critical hot spots.

C. System Characteristics

The proposed system incorporates hybrid spintronic/CMOS devices. The spintronic circuit is based on an MTJ. An MTJ is a structure composed of two ferromagnetic (FM) layers separated by an insulator barrier [13]. The resistance of the device is controlled by the difference in the magnetization angle between the two layers. The device exhibits two stable states, a parallel (P) state (where the two layers are

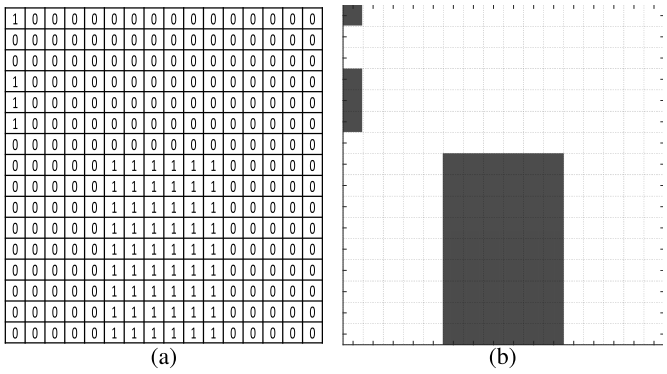

Fig. 5. 16×16 thermal map. (a) Output sensor node readings. (b) Thermal map. The dark areas represent nodes with a temperature above the temperature threshold.

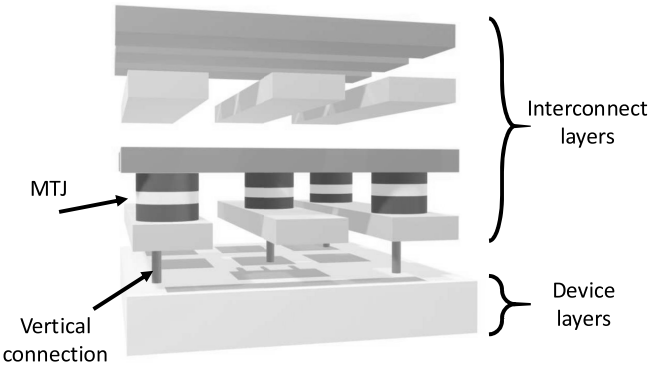

Fig. 6. MTJ, interconnect, and device layers.

magnetized in the same direction) and an AP state [14]. The MTJ is combined with CMOS to provide an efficient temperature-sensing element. An MTJ/CMOS-based thermal sensor exhibits small size, low power, high linearity, and high sensitivity [15]. These capabilities support a thermal-aware system composed of hundreds of distributed thermal sensor nodes.

The MTJ is integrated between the metallic layers above the CMOS device layers, as shown in Fig. 6, making this structure a good candidate for a local, distributed thermal sensor. MTJ fabrication is sufficiently mature for different technology platforms such as bulk-CMOS, FDSOI-CMOS, and FINFET CMOS [16]. Intel [17], GlobalFoundries [18], Samsung [19], and other large foundries are integrating MTJ technology with CMOS at different technology nodes. These advancements in fabrication can produce high-quality MTJs for thermal sensing applications. In addition, MTJ memory can operate over a wide range of temperatures, -40 °C to 125 °C, in a stable manner for commercial, automotive, and military applications [20]. The ability of MTJ technology to be integrated with CMOS, operate over a wide, stable temperature range, and exhibit almost zero leakage current in the off state, with higher temperature sensitivity than conventional CMOS devices suggests an MTJ/CMOS temperature sensor is an effective candidate for next generation thermal-aware systems [15].

The use of an MTJ as a thermal sensor is supported by the high thermal sensitivity of the MTJ AP resistance.

The resistance of an MTJ changes almost linearly with high sensitivity with temperature in the AP state (as compared to the parallel state) [21]–[24]. The sensitivity of an MTJ to temperature is proposed in multiple MTJ structures such as CoFeB/Al-O/CoFeB [21], [22], Fe/MgO/Fe [23], and CoFeB/MgO/CoFeB [24]. The thermal sensitivity of the MTJ AP resistance depends upon the device material structure, dimensions, and applied sense voltage.

The proposed temperature sensor cell is discussed in Section III. The physical, magnetic, and electrical behavior of an MTJ in addition to the proposed thermal sensor are reviewed. A comparison between the proposed temperature sensor and conventional CMOS sensors in terms of sensitivity, linearity, power consumption, and area is also provided.

III. Integrated Solutions for Thermal Monitoring

A variety of CMOS-based integrated electronic devices and circuits can produce a thermal response [25]. The most commonly used temperature sensor is the Brokaw bandgap circuit where a voltage or current produces a proportional-to-absolute temperature (PTAT) relationship [26], [27]. This circuit requires at least two large bipolar transistors to extract the PTAT signal. Other thermal sensors are based on a change in the threshold voltage of the diode or transistor with temperature [28]. This change in threshold voltage with temperature is exponential, requiring additional circuitry such as a threshold voltage extractor circuit [28] or lookup table [29] to accurately predict the temperature. Drawbacks of these technologies are high leakage currents, large device capacitance (which influences the circuit response), poor stability, and low sensitivity over a wide temperature range with thermal cycling [4]. The need for calibration prior to use and low sensitivity with device scaling are also common issues [4]. A spintronic device—the MTJ—is therefore suggested as a thermal sensing element for large scale distributed systems.

For an MTJ, the temperature influences the device magnetic anisotropy, AP resistance, charge magnetic polarization, and thermal induced magnetic field [30]. The influence of both the sense voltage and temperature on an MTJ is discussed in Section III-A. A comparison between four thermal sensors (a diode connected transistor, two paired transistors, a hybrid MTJ/transistor, and a hybrid MTJ/transistor with an active load) is described in Section III-B.

A. MTJ as an Integrated Thermal Sensor

A macrospin model, described in the Appendix, is used here. The model includes the influence of the sense voltage and temperature on the device tunneling magnetoresistance $\mathrm{TMR}(T, V)$, layer spin polarization $P(T)$, saturation magnetization $M_S(T)$, device magnetic anisotropy constant $K(T)$, and voltage-controlled magnetic anisotropy (VCMA) constant $\zeta_{\mathrm{VCMA}}(T)$.

The influence of temperature on the conductance of an MTJ is the sum of two components, as described by (A.3): a spin-dependent (elastic) term due to the thermal excitation of the spin polarized electrons and a spin-independent term

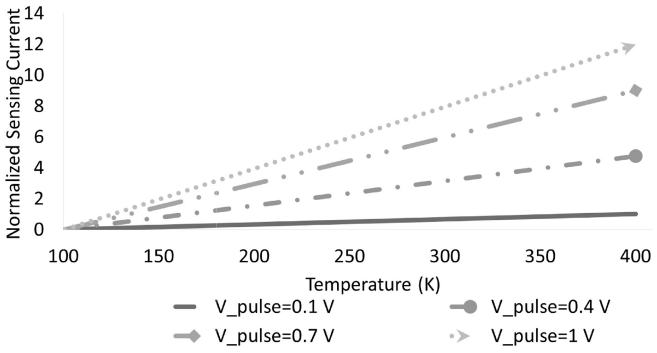

Fig. 7. Normalized sensing current of AP MTJ at different sense voltages [30].

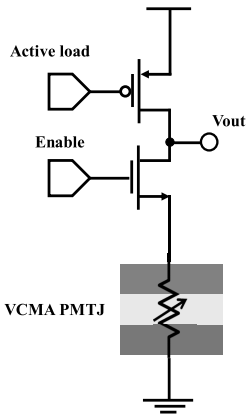

Fig. 8. Proposed MTJ/CMOS-based thermal sensor.

(inelastic) due to scattering by defects and impurity states. The device AP resistance decreases with increasing temperature. Under different sense voltages, the device exhibits a different sensitivity rate, as shown in Fig. 7.

The sensing technique considers the effects of temperature and sense voltage on the thermal stability and resistance of an MTJ. Hence, an MTJ operates in the stable AP state despite fluctuations in operating temperature and supply voltage. The thermal stability Δ of an MTJ determines the limits of the applied voltage and range of temperature over which the device can stably operate without switching [30]. Δ is the ratio of the magnetization energy of an MTJ and the thermal perturbation to the system, which is a function of temperature and applied voltage

$$\Delta(T, V) = \frac{\Delta E(T, V)|_{\mathrm{MTJ}}}{K_{\mathrm{B}}T} = \frac{K_{\mathrm{eff}}(T, V)\nu_{\mathrm{FM}}}{K_{\mathrm{B}}T} \tag{1}$$

where K_{B} is the Boltzmann's constant, $\Delta E(T, V)|_{\mathrm{MTJ}}$ is the system anisotropy energy of an MTJ, K_{eff} is the effective anisotropy constant, and ν_{FM} is the volume of the FM layer. An MTJ with a high thermal stability factor is required for thermal sensing applications. An MTJ with a high thermal stability of 279 is achieved [31].

The proposed MTJ-based thermal sensor is illustrated in Fig. 8, where a common source amplifier with a PMOS current source behaves as an active load. The active load bias and device size determine the circuit sensitivity. The

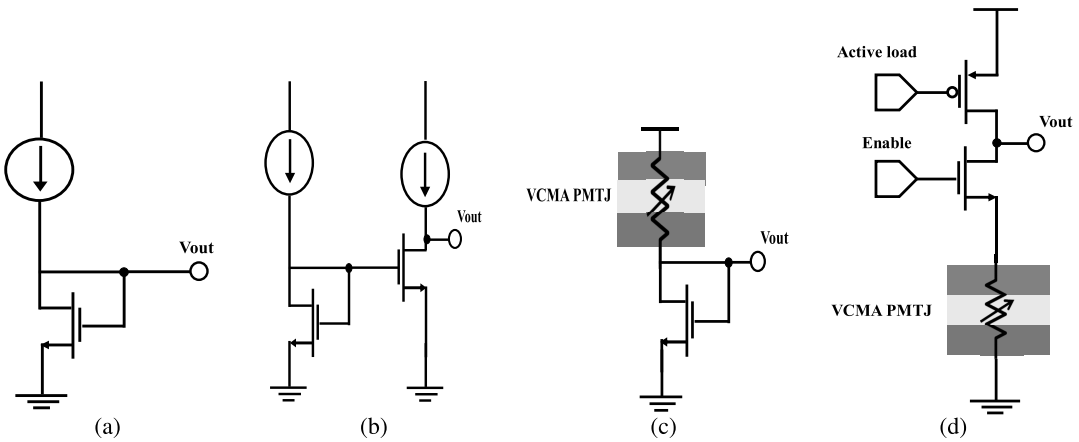

Fig. 9. Sensors. (a) Diode-connected transistor. (b) Two paired transistors. (c) Hybrid MTJ/transistor. (d) Hybrid MTJ/transistor with an active load.

TABLE I
COMPARISON OF THE PROPOSED TEMPERATURE SENSOR AND CONVENTIONAL CMOS SENSORS IN TERMS OF SENSITIVITY, LINEARITY, POWER CONSUMPTION, AND AREA

		Circuit (a)	Circuit (b)	Circuit (c)	Circuit (d)
Sensitivity (mV/K)	Commercial (0: 85)	0.51	0.51	0.4	1.91
	Industrial (-40:100)	1.03	1.03	0.64	3.78
	Automotive (-40:125)	1.08	1.08	0.77	3.97
	Military (-55:125)	1.35	1.35	0.81	4.8
Linearity	Commercial (0: 85)	0.985	0.985	1	0.983
	Industrial (-40:100)	0.953	0.953	0.999	0.96
	Automotive (-40:125)	0.941	0.941	0.999	0.947
	Military (-55:125)	0.919	0.919	0.996	0.936
Power Consumption@RT 27°C(μW)		40	80	18	11.9
Area (μm^2)		4X	8X	1X	2X

increase in circuit sensitivity and linearity with temperature is compared in Section III-B with CMOS-only thermal sensors.

B. Comparison With Conventional Integrated Solutions

A hybrid MTJ/CMOS-based thermal sensor is proposed in this article. The circuit considers the influence of temperature on both the threshold voltage of the transistor and the AP resistance of the MTJ. A comparison between four different circuits clarifies the advantages of an MTJ combined with a CMOS device. The circuits are shown in Fig. 9.

Circuits (a) and (b) are CMOS-only thermal sensors, where Circuit (a) is a diode-connected transistor thermal sensor biased by a current source, and Circuit (b) is the same as Circuit (a) followed by a common source amplifier stage. In Circuit (b), the two transistors perform temperature sensing, which enhances the stability and linearity with temperature. Circuits (c) and (d) are MTJ/CMOS-based thermal sensors.

A comparison of these sensors is listed in Table I. The simulation results are based on the MTJ macrospin compact model [30] of a VCMA PMTJ and the predictive transistor model (16-nm PTM) for CMOS transistors [32]. The CMOS transistors are sized the same (32 nm $\times$ 16 nm) and biased at the same current (31 nA) to establish a fair comparison.

The two CMOS-only thermal sensors, Circuits (a) and (b), exhibit good sensitivity with reasonable linearity. CMOS-only thermal sensors exhibit low linearity with temperature due to the exponential change in threshold voltage with respect to temperature. Incorporating an MTJ with CMOS increases the linearity of the thermal sensor, as listed in Table I, where Circuits (c) and (d) exhibit higher linearity than CMOS-only thermal sensors. To increase the sensitivity of MTJ/CMOS-based thermal sensors, Circuit (d) is proposed where the active load voltage biases the circuit at the highest sensitivity and linearity. The sensitivity and linearity of the MTJ/CMOS thermal sensors outperform the CMOS-only thermal sensors due to the high linearity of the MTJ response to temperature.

In terms of power consumption, Circuit (d) exhibits the lowest power consumption since this sensor does not require additional current and uses the lowest on-current in comparison to the other sensors for the same supply voltage. The MTJ/CMOS-based thermal sensor is smaller since no current source is required.

As listed in Table I, Circuit (d) exhibits the highest sensitivity and lowest power consumption. Circuit (d) is, therefore, considered as a system-wide temperature sensor in the proposed thermal-aware system. In Section IV, simulation results of the proposed system incorporating the hybrid MTJ/transistor thermal sensor node are presented. A comparison between the proposed thermal-aware system in terms of energy consumption, delay, and system size is also described.

IV. SIMULATION RESULTS

The system operation works as follows. The sense amplifier sets the sensor node voltage. Based on the grid size and number of nodes, preamplifier stages or buffers increase the current, enhance the sensitivity, and isolate the sensor node signal. The signal path of the sensor node to the output, as shown in Fig. 10, is used to characterize system performance. The system characteristics are listed in Table II, where the power consumption includes the energy consumed in the sensor nodes, buffers, inverters, amplifiers, and decoder. The delay of the read operation is the time required to read each of the rows.

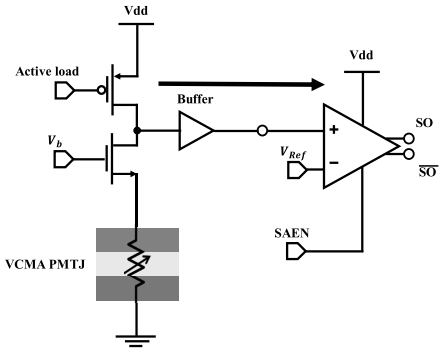

Fig. 10. Sensor signal path.

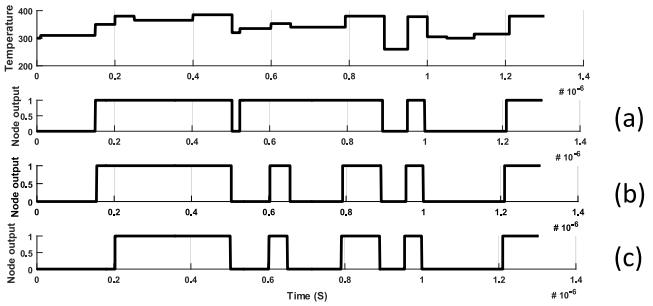

Fig. 11. System output. (a) $V_{\text{ref}} = 300$ mV which maps to a threshold temperature of $T = 332$ K. (b) $V_{\text{ref}} = 304$ mV and $T = 343$ K. (c) $V_{\text{ref}} = 306$ mV and $T = 350$ K.

TABLE II
CHARACTERISTICS OF THE DISTRIBUTED THERMAL NETWORK FOR DIFFERENT GRID SIZES

System size	Energy consumption (pJ)	Relative path delay to read the grid w.r.t. 4 × 4	System size #	
			Transistors	MTJs
4 × 4	1.32	1x	90	16
8 × 8	8.96	2x	304	64
16 × 16	65.50	4x	1,120	256
32 × 32	499	8x	4,980	1024

TABLE III
COMPARISON BETWEEN THE CMOS/MTJ THERMAL SENSOR SYSTEM AND [12]

	Proposed thermal aware system	[12]
Sensing Scheme	Change in AP resistance to temperature	Change in probability of switching
Sensor node	One MTJ, two transistors, V_{dd}	Two MTJs, two transistors, V_{dd}, I_{bias}
System Requirement	Latch-based amplifier	Circuit to map probability of switching an MTJ to temperature
Energy	0.5 nJ (To read network of 32 × 32 cells)	8.5 nJ
Accuracy	3 K	1 K
Output	1 or 0 indicating above or below threshold temperature	Local temperature

A read pulse of 1 ns is used to produce an output decision of one sensor node. The comparator delay is 0.03 ns. The accuracy of the system temperature is ±3 K for a reference voltage with an accuracy of ±1 mv. The area of each sensor node is 32 nm × 64 nm where the MTJ layer is between the second and third interconnect layers, as shown in Fig. 6. The average sense current of a thermal sensor node is 11 μA. The sensor nodes need to be calibrated prior to use due to the influence of manufacturing process variations. Different calibration schemes of multiple on-chip thermal sensors have been proposed [4]. The design, management, and control of these thermal sensors are the foci of this article. The ability to fabricate an MTJ with a different AP resistance (thermal sensitivity) has been achieved [23], and additional research is required to enhance the sensitivity of an MTJ to thermal and process variations.

An example of the system output at three different reference voltages, 300, 304, and 306 mV, mapped to, respectively, threshold temperatures of 332, 343, and 350 K is shown in Fig. 11. A multiplexer can be added to switch the reference signal between different voltages to vary the threshold temperature of the sensor nodes.

A comparison between the proposed hybrid CMOS/MTJ thermal sensor and the circuit described in [12] in terms of system requirements, sensing scheme, energy, read accuracy, and temperature range is listed in Table III. The primary purpose of this article is to describe a hybrid MTJ/CMOS-based thermal sensor and a related thermal-aware system. A distributed thermal sensor network able to provide an updated spatial and temporal thermal map in real time is also described in this article.

The proposed system provides flexibility in choosing a threshold temperature. The system can also support a multithreshold sensing scheme. This capability can be achieved by multiplexing the reference voltage. At each reference voltage, the system identifies whether the temperature at a sensor node is above or below a certain threshold temperature. As an example, with two different reference voltages, the system could identify the temperature at a sensor node within three different temperature regions (below $T1$, between $T1$ and $T2$, or above $T2$).

With hundreds of on-chip thermal sensor nodes distributed across a system, the ability to monitor local heat (characterizing the generated heat and thermal paths) is achieved. This capability for real-time spatial and temporal sensing provides significant information characterizing the thermal behavior which can be used to mitigate on-chip heat generation and distribution issues.

V. CONCLUSION

The need for a thermal-aware system increases with device scaling and the size of the integrated system. A thermal-aware system is proposed where a grid structure is composed of individual thermal sensor cells. The sensor nodes are based on hybrid spintronic/CMOS technology, where the AP resistance of an MTJ exhibits a thermal linearity of 0.9 and thermal sensitivity of 4.8 mV/K over a temperature range of −55 °C to 125 °C. A system of 1045 thermal sensors distributed in a 32 × 32 grid structure consumes approximately 500 pJ. This low energy and high sensitivity are appropriate for next-generation thermal-aware systems.

TABLE IV
MTJ PHYSICAL PARAMETERS

Parameters	Description	Value
w_{FL}	FM width = radius	20 nm
t_{FL}	FM thickness	1.5 nm
t_{ox}	Barrier thickness	1.1 nm
Φ_{BL}	Barrier height	0.39 eV
V_h	Voltage @ half TMR	0.5 V
S	Spin independent conductance factor	1.1×10^{-12}
β_P	Fitting parameter for P	2.07×10^{-5}
α_P	Fitting parameter for P	2.3
β_M	Fitting parameter for M_S	1.5
T^*	Fitting parameter	1120 K
β_{Ki}	Fitting parameter	2.3
$\beta_{\xi VCMA}$	Fitting parameter	2.83
N_z	Demagnetization tensor factor in Z	0.9343
N_{xy}	Demagnetization tensor factor in XY	0.015
K_{i0}	Interfacial MA at 0 K	$2.02 \times 10^{-3} J/m^2$
M_{S0}	Saturation magnetization at 0 K	$1457 \times 10^3 A/m$
TMR_0	TMR at 0 K	3
ξ_{VCMA0}	VCMA factor at 0 K	48.9×10^{-15} J/(V.m)

APPENDIX
MTJ MACROSPIN MODEL

A macrospin compact model which characterizes a VCMA MgO|CoFeB perpendicular MTJ is described here [30]. The model considers the dynamic response of the device magnetic and electrical performance. The magnetization dynamics of the free FM layer are described by the modified Landau–Lifshitz–Gilbert equation. This expression describes the dynamic magnetic behavior of the FM layer as

$$\frac{\partial \vec{M}}{\partial t} = -\frac{\gamma\, \mu_o}{1+\alpha^2}\left[\vec{M} \times \vec{H}_{\text{eff}} + \alpha\ \vec{M} \times \frac{\partial \vec{M}}{\partial t}\right] + \gamma\ \sum \vec{\tau}_i \tag{A.1}$$

where $\vec{M}$ is the normalized free layer magnetization, t is the time variable, $\vec{H}_{\text{eff}}$ is the effective magnetic field expressed in A/m, γ is the electron gyromagnetic ratio, $\gamma \approx -2\pi \times 27.99$ GHz/T, μ_{o} is the permeability of free space, α is the Gilbert damping factor, and $\vec{\tau}_{\text{i}}$ is the applied torque due to other perturbations such as current which exerts a spin transfer torque [33].

The macrospin model is developed in association with the static and dynamic micromagnetic analyses of the system energy. The applied effective magnetic field to the free layer $\vec{H}_{\text{eff}}$ is

$$\vec{H}_{\text{eff}} = \vec{H}_{\text{UA}} - \vec{H}_{\text{dem}} + \vec{H}_c + \vec{H}_{\text{ext}} - \vec{H}_{\text{VCMA}} + \vec{H}_{\text{th}} \tag{A.2}$$

where $\vec{H}_{\text{UA}}$ is the uniaxial anisotropy field sometimes defined as $\vec{H}_K$, $\vec{H}_{\text{dem}}$ is the demagnetization field, $\vec{H}_{\text{c}}$ is the coupling field due to the other FM layer, $\vec{H}_{\text{ext}}$ is the applied external magnetic field, $\vec{H}_{\text{VCMA}}$ is due to VCMA, and $\vec{H}_{\text{th}}$ is the stochastic magnetic field due to thermal variations.

The MTJ AP conductance is modeled as [34]

$$G_{\text{AP}}(T) = G_{\text{T}}[1 - P_1(T)P_2(T)] + G_{\text{SI}} \tag{A.3}$$

where $G_{\text{T}} = G_0\ (\sin(CT)/\text{CT})$ is the thermal smearing factor, $G_0 = (3.16 \times 10^{10}\sqrt{\phi_{\text{B}}}/t_{\text{ox}})\exp(-1.025 \times \sqrt{\phi_{\text{B}}} \times t_{\text{ox}})$ is the parallel state conductance at zero voltage and zero temperature, T is the ambient temperature, ϕ_{B} is the average tunneling barrier height (in eV), t_{ox} is the thickness of the insulator barrier layer, and $C = 1.387 \times 10^{-4} t_{\text{ox}}/\sqrt{\phi_{\text{B}}}$ is a material-dependent parameter [34]. $G_{\text{SI}} = \text{ST}^{4/3}$ is the inelastic spin-independent conductance, and S is a fitting parameter. P_1 and P_2 are the spin polarization percentage of the two FM layers. The dependence of the spin polarization on temperature can be fit as [21], [35]

$$P(T) = P(0)[1 - \beta_P T^{\alpha_P}\ ] \tag{A.4}$$

where β_{P} and α_{P} are the fitting parameters related to the device dimensions and material properties.

The physical parameters are based on perpendicular magnetic anisotropy and VCMA MgO|CoFeB [30], [36], [37]. The experimentally extracted model parameters are listed in Table IV.

REFERENCES

[1] U. Monga *et al.*, "Impact of self-heating in SOI FinFETs on analog circuits and interdie variability," *IEEE Electron Device Lett.*, vol. 32, no. 3, pp. 249–251, Mar. 2011.

[2] Y. Fu *et al.*, "Thermal sensor placement and thermal reconstruction under Gaussian and non-Gaussian sensor noises for 3-D NoC," *IEEE Trans. Comput.-Aided Design Integr.*, vol. 38, no. 11, pp. 2139–2152, Nov. 2019.

[3] B. Vaisband, I. Savidis, and E. G. Friedman, "Thermal conduction path analysis in 3-D ICs," in *Proc. IEEE Int. Symp. Circuits Syst. (ISCAS)*, Jun. 2014, pp. 594–597.

[4] C. Yao, K. K. Saluja, and P. Ramanathan, "Calibrating on-chip thermal sensors in integrated circuits: A design-for-calibration approach," *J. Electron. Test.*, vol. 27, no. 6, pp. 711–721, Dec. 2011.

[5] M. Malits and Y. Nemirovsky, "Nanometric integrated temperature and thermal sensors in CMOS-SOI technology," *Sensors*, vol. 17, no. 8, p. 1739, Jul. 2017.

[6] M. Mansoor, I. Haneef, S. Akhtar, A. De Luca, and F. Udrea, "Silicon diode temperature sensors—A review of applications," *Sens. Actuators A, Phys.*, vol. 232, pp. 63–74, Aug. 2015.

[7] M. S. Floyd *et al.*, "System power management support in the IBM POWER6 microprocessor," *IBM J. Res. Develop.*, vol. 51, no. 6, pp. 733–746, Nov. 2007.

[8] H. F. Sheikh, I. Ahmad, Z. Wang, and S. Ranka, "An overview and classification of thermal-aware scheduling techniques for multi-core processing systems," *Sustain. Comput., Inform. Syst.*, vol. 2, no. 3, pp. 151–169, Sep. 2012.

[9] A. Das, G. V. Merrett, M. Tribastone, and B. M. Al-Hashimi, "Workload change point detection for runtime thermal management of embedded systems," *IEEE Trans. Comput.-Aided Design Integr.*, vol. 35, no. 8, pp. 1358–1371, Aug. 2016.

[10] K.-C. Chen, Y.-H. Chen, and Y.-P. Lin, "Thermal sensor allocation and full-system temperature characterization for thermal-aware mesh-based NoC system by using compressive sensing technique," in *Proc. Int. Symp. VLSI Design, Autom. Test (VLSI-DAT)*, Apr. 2017, pp. 1–4.

[11] Y. S. Chung, R. W. Baird, and M. A. Dulram, "Magnetic tunnel junction temperature sensors and methods," U.S. Patent 7 510 883, Mar. 31, 2009.

[12] A. Sengupta, C. M. Liyanagedera, B. Jung, and K. Roy, "Magnetic tunnel junction as an on-chip temperature sensor," *Sci. Rep.*, vol. 7, no. 1, Dec. 2017, Art. no. 11764.

[13] M. Julliere, "Tunneling between ferromagnetic films," *Phys. Lett. A*, vol. 54, no. 3, pp. 225–226, Sep. 1975.

[14] J. C. Slonczewski, "Current-driven excitation of magnetic multilayers," *J. Magn. Magn. Mater.*, vol. 159, nos. 1–2, pp. L1–L7, Jun. 1996.

[15] A. G. Qoutb and E. G. Friedman, "Spintronic/CMOS-based thermal sensors," in *Proc. IEEE Int. Symp. Circuits Syst.*, to be published.

[16] Y. K. Lee *et al.*, "Embedded STT-MRAM in 28-nm FDSOI logic process for industrial MCU/IoT application," in *Proc. IEEE Symp. VLSI Technol.*, Jun. 2018, pp. 181–182.

[17] H.-J. Lee *et al.*, "Intel 22nm FinFET (22FFL) process technology for RF and mmWave applications and circuit design optimization for FinFET technology," in *IEDM Tech. Dig.*, Dec. 2018, pp. 14.1.1–14.1.4.

[18] J. H. Lim *et al.*, "Investigating the statistical-physical nature of MgO dielectric breakdown in STT-MRAM at different operating conditions," in *IEDM Tech. Dig.*, Dec. 2018, pp. 25.3.1–25.3.4.

[19] Y. J. Song *et al.*, "Demonstration of highly manufacturable STT-MRAM embedded in 28 nm logic," in *IEDM Tech. Dig.*, Dec. 2018, pp. 18.2.1–18.2.4.

[20] J. Heidecker, "MRAM technology status: NASA electronic parts and packaging (NEPP) program office of safety and mission assurance," Jet Propuls. Lab., NASA, Pasadena, CA, USA, Tech. Rep., Feb. 2013.

[21] L. Yuan, S. H. Liou, and D. Wang, "Temperature dependence of magnetoresistance in magnetic tunnel junctions with different free layer structures," *Phys. Rev. B, Condens. Matter*, vol. 73, no. 13, Apr. 2006, Art. no. 134403.

[22] Z. M. Zeng, Y. Wang, X. F. Han, W. S. Zhan, and Z. Zhang, "Bias voltage and temperature dependence of magneto-electric properties in double-barrier magnetic tunnel junction with amorphous Co-Fe-B electrodes," *Eur. Phys. J. B*, vol. 52, no. 2, pp. 205–208, Jul. 2006.

[23] Q. L. Ma *et al.*, "Temperature dependence of resistance in epitaxial Fe/MgO/Fe magnetic tunnel junctions," *Appl. Phys. Lett.*, vol. 95, no. 5, Aug. 2009, Art. no. 052506.

[24] A. A. Khan *et al.*, "Elastic and inelastic conductance in Co-Fe-B/MgO/Co-Fe-B magnetic tunnel junctions," *Phys. Rev. B, Condens. Matter*, vol. 82, no. 6, Aug. 2010, Art. no. 064416.

[25] K. Makinwa. *Smart Temperature Sensor Survey*. Accessed: Mar. 1, 2019. [Online]. Available: http://ei.ewi.tudelft.nl/docs/TSensor_survey.xls

[26] A. P. Brokaw, "A temperature sensor with single resistor set-point programming," in *IEEE Int. Solid-State Circuits Conf. Dig. Tech. Papers*, Feb. 1996, pp. 334–335.

[27] A. Bakker and J. H. Huijsing, "Micropower CMOS temperature sensor with digital output," *IEEE J. Solid-State Circuits*, vol. 31, no. 7, pp. 933–937, Jul. 1996.

[28] M. Malits, I. Brouk, and Y. Nemirovsky, "Study of CMOS-SOI integrated temperature sensing circuits for on-chip temperature monitoring," *Sensors*, vol. 18, no. 5, p. 1629, May 2018.

[29] J. Cui and D. L. Maskell, "A fast high-level event-driven thermal estimator for dynamic thermal aware scheduling," *IEEE Trans. Comput.-Aided Design Integr.*, vol. 31, no. 6, pp. 904–917, Jun. 2012.

[30] A. G. Qoutb and E. G. Friedman, "PMTJ temperature sensor utilizing VCMA," in *Proc. IEEE Int. Symp. Circuits Syst. (ISCAS)*, May 2019, pp. 1–5.

[31] R. Heindl, A. Chaudhry, and S. E. Russek, "Estimation of thermal stability factor and intrinsic switching current from switching distributions in spin-transfer-torque devices with out-of-plane magnetic anisotropy," *AIP Adv.*, vol. 8, no. 1, Jan. 2018, Art. no. 015011.

[32] *Predictive Technology Model (PTM)*. Accessed: Mar. 1, 2019. [Online]. Available: http://ptm.asu.edu/

[33] T. L. Gilbert and H. Ekstein, "Basis of the domain structure variational principle," *Bull. Amer. Phys. Soc.*, vol. 1, p. 25, 1956.

[34] W. F. Brinkman, R. C. Dynes, and J. M. Rowell, "Tunneling conductance of asymmetrical barriers," *J. Appl. Phys.*, vol. 41, no. 5, pp. 1915–1921, Apr. 1970.

[35] C. H. Shang, J. Nowak, R. Jansen, and J. S. Moodera, "Temperature dependence of magnetoresistance and surface magnetization in ferromagnetic tunnel junctions," *Phys. Rev. B, Condens. Matter*, vol. 58, no. 6, pp. R2917–R2920, Aug. 1998.

[36] J. G. Alzate *et al.*, "Temperature dependence of the voltage-controlled perpendicular anisotropy in nanoscale MgO|CoFeB|Ta magnetic tunnel junctions," *Appl. Phys. Lett.*, vol. 104, no. 11, Mar. 2014, Art. no. 112410.

[37] L. Zhang *et al.*, "Addressing the thermal issues of STT-MRAM from compact modeling to design techniques," *IEEE Trans. Nanotechnol.*, vol. 17, no. 2, pp. 345–352, Mar. 2018.